

# Spectral variability of the particulate backscattering ratio

A. L. Whitmire<sup>1</sup>, E. Boss<sup>2</sup>, T. J. Cowles<sup>1</sup>, and W. S. Pegau<sup>3</sup>

<sup>1</sup>College of Oceanic & Atmospheric Sciences, Oregon State University, Corvallis, Oregon 97331

<sup>2</sup>School of Marine Sciences, University of Maine, 458 Aubert Hall, Orono, ME 04469

<sup>3</sup>School of Marine Sciences, University of Maine, 458 Aubert Hall, Orono, ME 04469

<sup>3</sup>Oil Spill Recovery Institute, P.O. Box 705, Cordova, AK 99574

[abriggs@coas.oregonstate.edu](mailto:abriggs@coas.oregonstate.edu), [tjc@coas.oregonstate.edu](mailto:tjc@coas.oregonstate.edu)

[emmanuel.boss@maine.edu](mailto:emmanuel.boss@maine.edu)

[wspgau@pwssc.gen.ak.us](mailto:wspgau@pwssc.gen.ak.us)

**Abstract:** The spectral dependency of the particulate backscattering ratio is relevant in the fields of ocean color inversion, light field modeling, and inferring particle properties from optical measurements. Aside from theoretical predictions for spherical, homogeneous particles, we have very limited knowledge of the actual *in situ* spectral variability of the particulate backscattering ratio. This work presents results from five research cruises that were conducted over a three-year period. Water column profiles of physical and optical properties were conducted across diverse aquatic environments that offered a wide range of particle populations. The main objective of this research was to examine the behavior of the spectral particulate backscattering ratio *in situ*, both in terms of its absolute magnitude and its variability across visible wavelengths, using over nine thousand 1-meter binned data points for each of five wavelengths of the spectral particulate backscattering ratio. Our analysis reveals no spectral dependence of the particulate backscattering ratio within our measurement certainty, and a geometric mean value of 0.013 for this dataset. This is lower than the commonly used value of 0.0183 from Petzold's integrated volume scattering data. Within the first optical depth of the water column, the mean particulate backscattering ratio was 0.010.

© 2007 Optical Society of America

**OCIS codes:** (010.4450) Ocean optics; (290-1350) Backscattering; (290-5850) Scattering, particles

---

## References and Links

1. C. D. Mobley, L. K. Sundman, and E. Boss, "Phase function effects on oceanic light fields," *Appl. Opt.* **41**, 1035-1050 (2002).
2. H. R. Gordon, and A. Morel, "Remote Assessment of Ocean Color for Interpretation of Satellite Visible Imagery: A Review," R. T. Barber, C. N. K. Mooers, M. J. Bowman, and B. Zeitzschel, eds. (Springer-Verlag, New York, 1983).
3. D. Stramski, E. Boss, D. Bogucki, and K. J. Voss, "The role of seawater constituents in light backscattering in the ocean," *Prog. Oceanogr.* **61**, 27-56 (2004).
4. H. R. Gordon, O. B. Brown, R. H. Evans, J. W. Brown, R. C. Smith, K. S. Baker, and D. K. Clarks, "A semianalytic radiance model of ocean color," *J. Geophys. Res.* **93**, 10,909-10,924 (1988).
5. A. Morel, "Optical modeling of the upper ocean in relation to its biogenous matter content (Case I waters)," *J. Geophys. Res.* **93**, 10,749 - 10,768 (1988).
6. M. S. Twardowski, E. Boss, J. B. Macdonald, W. S. Pegau, A. H. Barnard, and J. R. V. Zaneveld, "A model for estimating bulk refractive index from the optical backscattering ratio and the implications for understanding particle composition in case I and case II waters," *J. Geophys. Res.* **106**, 14,129-14,142 (2001).
7. E. Boss, W. S. Pegau, M. Lee, M. S. Twardowski, E. Shybanov, G. Korotaev, and F. Baratange, "The particulate backscattering ratio at LEO-15 and its use to study particle composition and distribution," *J. Geophys. Res.* **109**, C0101410.1029/2002JC001514 (2004).

8. E. Aas, "Refractive index of phytoplankton derived from its metabolite composition," *J. Plankt. Res.* **18**, 2223-2249 (1996).
9. K. L. Carder, P. R. Betzer, and D. W. Eggimann, "Physical, chemical, and optical measures of suspended particle concentrations: their intercomparison and application to the West African shelf," in *Suspended Solids in Water*, R. J. Gibbs, ed., (Plenum, New York, 1974) pp. 173– 193.
10. J. M. Sullivan, M. S. Twardowski, P. L. Donaghay, and S. A. Freeman, "Use of optical scattering to discriminate particle types in coastal waters," *Appl. Opt.* **44**, 1667-1680 (2005).
11. O. Ulloa, S. Sathyendranath, and T. Platt, "Effect of the particle size-distribution on the backscattering ratio in seawater," *Appl. Opt.* **33**, 7070-7077 (1994).
12. J. B. Macdonald, M. S. Twardowski, W. S. Pegau, A. H. Barnard, E. Boss, and J. R. V. Zaneveld, "Characterization of spectral backscattering in the Gulf of California," in *EOS Trans. AGU*, **80**, *Ocean Sci. Mett. Suppl.* (2000).
13. M. Chami, E. B. Shybanov, T. Y. Churilova, G. A. Khomenko, M. E.-G. Lee, O. V. Martynov, G. A. Berseneva, and G. K. Korotaev, "Optical properties of the particles in the Crimea coastal waters (Black Sea)," *J. Geophys. Res.* **110**, doi:10.1029/2005JC003008 (2005).
14. D. McKee and A. Cunningham, "Evidence for wavelength dependence of the scattering phase function and its implication for modeling radiance transfer in shelf seas," *Appl. Opt.* **44**, 126-135 (2005).
15. E. Boss, R. Collier, G. Larson, K. Fennel, and W. S. Pegau, "Measurements of spectral optical properties and their relation to biogeochemical variables and processes in Crater Lake National Park, OR," *Hydrobiologia*, **574**, 149-159 (2007).
16. A. H. Barnard, W. S. Pegau, and J. R. V. Zaneveld, "Global relationships of the inherent optical properties of the oceans," *J. Geophys. Res.* **103**, 24,955 – 24,968, (1998).
17. W. S. Pegau, D. Gray, and J. R. V. Zaneveld, "Absorption and attenuation of visible and near-infrared light in the water: Dependence on temperature and salinity," *Appl. Opt.* **36**, 6035-6046 (1997).
18. J. R. V. Zaneveld, J. C. Kitchen, and C. C. Moore, "Scattering error correction of reflecting tube absorption meter," *Proc. SPIE* **2258**, 44-55 (1994).
19. R. F. Davis, C. C. Moore, J. R. V. Zaneveld, and J. M. Napp, "Reducing the effects of fouling on chlorophyll estimates derived from long-term deployments of optical instruments," *J. Geophys. Res.*, **102**, 5851-5855 (1997).
20. H. M. Sosik and B. G. Mitchell, "Light absorption by phytoplankton, photosynthetic pigments and detritus in the California Current System," *Deep Sea-Res.* **42**, 1717-1748 (1995).
21. R. A. Maffione and D. R. Dana, "Instruments and methods for measuring the backward-scattering coefficient of ocean waters," *Appl. Opt.* **36**, 6057-6067 (1997).
22. E. Boss and W. Scott Pegau, "The relationship of light scattering at an angle in the backward direction to the backscattering coefficient," *Appl. Opt.* **40**, 5503-5507 (2001).
23. T. Oishi, "Significant relationship between the backward scattering coefficient of sea water and the scatterance at 120 degrees," *Appl. Opt.* **29**, 4658-4665 (1990).
24. M. Chami, E. Marken, J. J. Starnes, G. Khomenko, and G. Korotaev, "Variability of the relationship between the particulate backscattering coefficient and the volume scattering function measured at fixed angles," *J. Geophys. Res.* **111**, doi:10.1029/2005JC003230 (2006).
25. W. S. Pegau, J. R. V. Zaneveld, and K. J. Voss, "Toward closure of the inherent optical properties of natural waters," *J. Geophys. Res.* **100**, 13,193–13,199 (1995).
26. T. J. Petzold, "Volume scattering functions for selected ocean waters," *SIO Ref. 72-78*, (Scripps Institution of Oceanography, 1972).
27. J. W. Campbell, "The lognormal distribution as a model for bio-optical variability in the sea," *J. Geophys. Res.* **100**, 13237-13254 (1995).
28. R. R. Sokal and F. J. Rohlf, *Biometry*, (W.H. Freeman and Company, New York, 1995).
29. E. T. Peltzer, "Matlab® shell-scripts for linear regression analysis," <http://www.mbari.org/staff/etp3/regressindex.htm> (9/18/2006).
30. E. Laws, *Mathematical Methods for Oceanographers* (John Wiley and Sons, New York, 1997).
31. Y.-H. Ahn, A. Bricaud, and A. Morel, "Light backscattering efficiency and related properties of some phytoplankters," *Deep-Sea Res. Part A* **39**, 1835–1855 (1992).
32. A. Bricaud, A. Morel, and L. Prieur, "Optical efficiency factors of some phytoplankters," *Limnol. Oceanogr.* **28**, 816-832 (1983).
33. A. Morel and S. Maritorena, Bio-optical properties of oceanic waters: A reappraisal. *Journal of Geophysical research*, **106**, 7763-7780 (2001).
34. H. R. Gordon, "Backscattering of light from disklike particles: is fine-scale structure or gross morphology more important?," *Appl. Opt.* **45**, 7166-7173 (2006).
35. J. C. Kitchen and J. R. V. Zaneveld, "A three-layered sphere model of the optical properties of phytoplankton," *Limnol. Oceanogr.* **37**, 1680-1690 (1992).
36. A. Bricaud, C. Roesler, and J. R. V. Zaneveld, "In situ methods for measuring the inherent optical properties of ocean waters," *Limnol. Oceanogr.* **40**, 393-410 (1995).
37. C. S. Roesler and E. Boss, "A novel ocean color inversion model: retrieval of beam attenuation and particle size distribution," *Geophys. Res. Lett.* **30**, 10.1029/2002GL016366 (2003).

## 1. Introduction

The spectral particulate backscattering ratio,  $\tilde{b}_{bp}(\lambda)$ , is the ratio of light scattered in the backward hemisphere to the total light scattered by a particle or group of particles. There are currently two primary applications for backscattering ratio data; inferring particle composition from *in situ* optical measurements, and modeling the *in situ* light field. In a study that used HYDROLIGHT to investigate the effects of the shape of the scattering phase function and the backscattering ratio on the underwater light field, Mobley et al. [1] found that using the correct backscattering ratio was crucial in obtaining closure between model and field data. They obtained closure in observed and modeled reflectance when using empirical or analytical phase functions that had the backscattering ratio observed in the field. Results were insensitive to the detailed volume scattering function [VSF] in the backward direction (90 – 180 degrees).

The spectral particulate backscattering ratio also has important applications in the interpretation of remote sensing data. To first order, the reflectance of the ocean,  $R$ , the ratio of upwelled radiance (or irradiance) to downwelled irradiance, is directly proportional to the ratio of backscattering to absorption ( $b_b(\lambda)$  and  $a(\lambda)$  respectively; [2]), which in turn depend upon the particulate and dissolved constituents of seawater. The absorption properties of marine substances have been well characterized through laboratory and field measurements, but major gaps exist in our understanding of the backscattering properties of marine substances [3]. As a result, many remote sensing algorithms estimate the particulate backscattering coefficient as the product of the backscattering ratio and the scattering coefficient. Radiance models for Case I waters have long assumed a backscattering probability between 0.2% and 2% depending on the chlorophyll concentration [4,5], but little *in situ* data has been available to test this assumption.

The backscattering ratio has also been used to infer particle properties *in situ*. The backscattering ratio, in concert with the slope of the particle size distribution, provides an estimate of the bulk refractive index of particles in the ocean, allowing discrimination between organically dominated particulate assemblages from those dominated by inorganic particles [6, 7]. This separation is a consequence of the larger water fraction in organic particles compared to inorganic particles, thus lowering their index of refraction [8]. This characteristic has significant ecological consequences since particulate sinking depends linearly on the particles' excess density relative to water, which correlates well with index of refraction [9]. When the spectral backscattering ratio is added to a suite of standard optical measurements (e.g. attenuation  $c(\lambda)$ , absorption  $a(\lambda)$ , and chlorophyll) more information is available to elucidate and track particle assemblages because the ratio often exhibits a different spatial distribution pattern than the other measurements [7,10]. For example, unlike measurements of  $c_p440$  and  $a_p676$ , the ratio may not resolve a high chlorophyll concentration at the surface due to the low index of refraction of most phytoplankton relative to water. The ratio could, however, strongly define the bottom boundary layer even when beam attenuation is low [see [7], Fig. 3]. This indicates that the distribution of the particulate backscattering ratio may offer information on the distribution of various particle populations in optically complex waters.

Due to the limited *in situ* data on the spectral dependence of the backscattering ratio for natural particles, it has been assumed to be spectrally flat as predicted by Mie theory [11]. MacDonald et al. [12] found less than 10% variability between wavelengths in their estimates of spectral particulate backscattering ratios. In a study conducted on a fixed platform in the Black Sea, Chami et al. [13] found that the mean particulate backscattering ratio had less than 4% variability between three wavelengths, but that significant deviations from a flat  $\tilde{b}_{bp}(\lambda)$  spectrum occurred under certain conditions. In a study conducted in the Irish and Celtic Seas, wavelength dependence was observed in the ratio between two wavelengths (470 and 676-

nm) under certain circumstances [14]. The discrepancies in the results of these studies illustrate the need for a more comprehensive investigation of the behavior of the spectral particulate backscattering ratio *in situ*. As yet, published results on the actual variability of *in situ* spectral particulate backscattering ratios do not cover a sufficiently wide range of water types and particle populations to justify the assumption of a flat backscattering ratio spectrum, and assumptions inherent in the Mie model (spherical, homogeneous particles that obey a Junge-type size distribution), limit its applicability in characterizing the scattering properties of marine particles. In addition, some of the above-mentioned works suffer from limitations; the 676-nm channel used in [14] is known to be sensitive to chlorophyll fluorescence at high chlorophyll concentrations as discussed in [15]. The sensor used in [13] is a prototype that has not benefited from review by a community of users.

In an effort to clarify this issue, we have analyzed five *in situ* data sets to explore the spectral dependence of the backscattering ratio using a commercially available sensor. We focused our analysis on describing the magnitude range of the backscattering ratio across many environments, and on differences in the ratio across visible wavelengths. We also investigated the effect of different biogeochemical domains on  $\tilde{b}_{bp}(\lambda)$ . We present over nine thousand 1-meter binned data points for each of five wavelengths of the spectral particulate backscattering ratio.

## 2. Methods

The data used in this paper were compiled from pre-existing datasets that had been collected and archived by the Optical Oceanography Group at Oregon State University [6, 7, 15]. The measurements were taken over a three-year period and cover diverse aquatic environments, offering a wide range of particle populations. Sampling sites included the region from the southern California coast to the Gulf of California, the mid-Atlantic Bight off the south coast of New Jersey, and Crater Lake, Oregon, USA. A summary of the dates and locations of these cruises is given in Table 1. Data were collected in various Case-1 and Case-2 waters ranging from near-shore coastal stations to oligotrophic and fresh-water environments. The variety of geographical locations and water types sampled offered a broad range of particle types and populations that spanned the expected range of the backscattering ratio. Note that the backscattering ratio depends on the properties of the particle assemblage, so the entire dynamic range of the particulate backscattering ratio may be observed in a single profile. The dataset does not cover all types of plankton assemblages (e.g. large, monospecific blooms), but does provide a very good representation of a broad range of mixed plankton populations, detritus composition, and lithogenic particles. We therefore believe that the results shown here are representative of the global oceans.

Table 1. Global Data Set Description

Location	Data Set	Dates	Latitude, °N	Longitude, °W	Number of Profiles	Number of Samples
Gulf of California	GOC99A	April – May 1999	24.4 – 31.1	114.6 – 108.8	36	2808
San Diego, CA to the Gulf of California	MOCE-5	October 1999	21.8 – 32.5	117.4 – 105.7	25	1854
Mid-Atlantic Bight	HY00	July – Aug. 2000	39.3 - 39.6	74.0 - 74.4	95	1054
Crater Lake	CL01	June and Sept.	42.93	122.1	4	766
Mid-Atlantic Bight	HY01	July – Aug. 2001	39.15 – 40.7	71.4 – 74.2	74	2672

Experiment abbreviations are as follows: GOC99A, Gulf of California, 1999; MOCE-5, Marine Optical Characterization Experiment, west coast of Baja, California and Gulf of California, 1999; HY00, Hyperspectral Coastal Ocean Dynamics Experiments (HyCODE), south New Jersey coast, 2000; CL01, Crater Lake, OR, 2001; HY01, HyCODE, south New Jersey coast, 2001. Total numbers of profiles and samples for the data set are 234 and 9,154, respectively.

## 2.1 Field methods

In all cases except for the Crater Lake cruise, water column profiles of physical and optical properties were collected with a Slow Descent Rate Optical Profiler (SlowDROP; [16]), a multi-instrument profiling system designed to freefall through the water column in order to isolate the profiler from ship motion. A SlowDROP package was unnecessary in the calm waters of Crater Lake, so standard winched profiles were conducted. The descent rate was on the order of 10's of centimeters per second, which enabled the capture of optical and hydrographic data on sub-meter scales [(O) 10cm]. A typical instrument configuration on the profiler included a CTD, a chlorophyll fluorometer, a six-wavelength backscattering sensor, and two nine-wavelength dual path absorption and attenuation meters, one of which had a 0.2 $\mu$ m pre-filter to measure the dissolved signal (operationally defined as the fraction smaller than 0.2 $\mu$ m).

## 2.2 Data correction and processing

*In situ* total and dissolved spectral absorption and attenuation were measured with two WET Labs *ac-9*'s at nine wavelengths; 412, 440, 488, 510, 532, 555, 650, 676, and 715-nm. Particulate absorption and attenuation were determined by the difference between the total and dissolved signals. To account for drift over the course of the cruises, daily field measurements of pure water were collected. Corrections for the temperature and salinity dependence of absorption and attenuation were also applied [17], as well as a correction for scattering losses in the absorption tube (proportional method) [18]. The scattering coefficient,  $b(\lambda)$ , was calculated as the difference between attenuation and absorption.

Chlorophyll concentration was estimated using the chlorophyll absorption line height technique [19, 15]. In this method the absorption due to chlorophyll-*a*,  $a_{chl}$ , is calculated using *ac-9* particulate absorption data at 650, 676, and 715-nm as follows:  $a_{chl} = a_p(676) - [39/65 \cdot a_p(650) + 26/65 \cdot a_p(715)]$ . The chlorophyll concentration is then estimated by normalizing  $a_{chl}$  by the chlorophyll-specific absorption coefficient,  $a^*(676)$ . We used an  $a^*(676)$  of 0.014 m<sup>2</sup> g chl<sup>-1</sup>, which is appropriate for oceanic waters dominated by phytoplankton [20]. This approach was utilized instead of estimating chlorophyll from fluorescence data to avoid the problem of non-photochemical quenching of fluorescence that occurs in surface waters under high light conditions. Previous work has shown this to be a robust technique, with an uncertainty in the chlorophyll estimate of  $\pm 0.2 \mu\text{g L}^{-1}$  [15, 10].

The HOBI Labs Hydrosat-6 (HS-6) instrument measures the total volume scattering function,  $\beta$ , at 140 degrees and six wavelengths [21]. The wavelengths used in our study were 442, 488, 532, 555, 620, and 676-nm. An extra correction step before the conversion to the backscattering coefficient was necessary for these data. HOBI Labs released a revised estimate of the reflectivity of the Spectralon target used during the Hydrosat calibration procedure after the data were collected, and volume scattering data were corrected by a factor of 1.12 to account for the revised reflectivity (D. Dana, personal communication, 2004). Derived parameters for the HS-6 include volume scattering by particles, and the total and particulate backscattering coefficients ( $\beta_p(\lambda)$ ,  $b_b(\lambda)$  and  $b_{bp}(\lambda)$  respectively) at six wavelengths [20]. All of the backscattering data were processed according to the procedures for conversion from  $\beta(\lambda, 140^\circ)$  to  $b_b(\lambda)$  that are discussed in Boss and Pegau [22], using a conversion factor,  $\chi$ , of 1.18.

Five out of six wavelengths in the HS-6 overlap with those of the *ac-9*, so particulate backscattering ratios were calculated directly as  $b_{bp}(\lambda)/b_p(\lambda)$  for those wavelengths. The *ac-9* does not have a 620-nm waveband, so  $b_p(620)$  was estimated by linear interpolation between  $b_p(555)$  and  $b_p(650)$ , and then the backscattering ratio was estimated using the result. We found that the data from the HS-6 676-nm waveband was significantly correlated with the chlorophyll concentration, which is likely the result of chlorophyll-*a* fluorescence excited at 676-nm and emitted at 681-nm [15]. The HS-6 676-nm waveband detector has a FWHM of 20

nm, which is sufficiently wide to detect chlorophyll-*a* fluorescence emission. Backscattering data from the 676-nm channel was therefore omitted from this analysis.

We used median values within 1-m depth bins for all variables, yielding a database of 10,513 data points for each IOP and hydrographic variable. The median was used instead of the mean because averages are sensitive to the presence of spikes caused by rare, large particles that may be observed by one instrument but not the other. Since rare particles are not normally distributed in time or space, excluding them through a median binning procedure minimizes their contribution to bias in the final data.

### 2.3 Uncertainties in the ratio

The particulate backscattering ratio, [ $\tilde{b}_{bp}(\lambda)$ ], was calculated as the quotient of the particulate backscattering coefficient ( $b_{bp}(\lambda)$  from the HS-6) and the particulate scattering coefficient ( $b_p(\lambda)$  from the *ac*-9). Propagation of error in each processing step for each instrument resulted in uncertainties of 0.0007 m<sup>-1</sup> and 0.006 m<sup>-1</sup> for the particulate backscattering coefficient and the particulate scattering coefficient respectively. Data less than or equal to the detection limit was excluded from our analysis. This reduced the dataset by 1,359 data points, or 13%, to a final size of 9,154 data points for each variable.

In addition to the above uncertainties, there is also an uncertainty associated with estimating the backscattering coefficient from a single angle measurement in the backward direction, which is estimated to be approximately 10% [22, 23, 24, 10]. Another possible source of uncertainty in the ratio is related to the acceptance angle of the *ac*-9's beam transmission detector [25]. Instruments that measure beam attenuation have to make a compromise between reducing the acceptance angle to exclude forward scattered light and enlarging the pinhole to maintain enough signal for a robust measurement. Up to 30% of the total volume scattering coefficient can occur in the range from 0 to 1 degree in natural waters [25]. The acceptance angle of the *ac*-9, 0.93 degrees, is large enough to accept some forward scattered light, especially when large particles are present. This would lead to an underestimate of the beam attenuation, and subsequently, the scattering coefficient. The end result in our application of *ac*-9 data would be an overestimate of the backscattering ratio.

The effect of the acceptance angle on the beam-*c* measurement has not been well characterized in the field. Based on Petzold's phase functions and the acceptance angle of the *ac*-9, we estimate a possible bias of 5-25% related to the uncertainty in the attenuation measurement when compared to theoretical calculations that do not take acceptance angle issue into account. The range in this estimate is due to the effect of particle size on the proportion of near-forward scattering. When more large particles are present the proportion of near-forward scattering relative to total scattering increases, and more scattered light is erroneously collected in the beam-*c* measurement. However, when compared to theoretical calculations where the acceptance angle is taken into account this bias is irrelevant [7]. Due to the uncertainty of the effect of the *ac*-9 acceptance angle on the attenuation measurement in our data, we do not include this possible bias in our estimates of error at this time.

Despite the different instruments and techniques that are used to estimate the backscattering ratio, prior work has demonstrated consistency between approaches (see Boss *et al.*, 2004 [7] for a review of instruments and methods). Intercalibration experiments to compare estimates of  $\tilde{b}_{bp}$  from different instruments and some of the data used here [7, 10, 15, 19] reveal that the ratio is a robust parameter with differences between instruments and methods on the order of 10%. Given that the instruments used for these comparisons measure the VSF at different angles, have very different calibration methods, and different methods of computing the backscattering ratio, an uncertainty of only 10% between them is remarkable. Using propagation of errors from the scattering and backscattering measurements, we set a conservative estimate of the likely maximum error of the particulate backscattering ratio

presented here to be 20%. This conservative estimate of error is greater than the estimate derived from the empirical studies mentioned above because we erred on the side of caution at each propagation step. Relative to the 4 to 10-fold variability of the backscattering ratio observed, a 20% maximum uncertainty in the estimate is not significant for most likely applications of the data (e.g. using it as a proxy for bulk particle composition). This is especially true given that the sources of error in the ratio (e.g. choice of  $\chi$ , acceptance angle of  $ac-9$ , measurement uncertainty) are not assumed to be spectrally dependent. Errors in our estimate of the ratio would affect all wavelengths similarly, and analyses of differences between the backscattering ratio at various wavelengths are therefore minimally influenced by even large uncertainties ((O) 20%).

### 3. Results

The frequency distributions of the particulate backscattering ratio for the combined dataset (all cruises pooled) at five wavelengths are shown in Fig. 1(A) – 1(E), and some parametric and non-parametric statistical descriptors are provided in Table 1. The ratios are clustered near zero and produce a distribution that is skewed to the right, with a skewness of 1.65. The geometric mean value of the ratio is 0.013, and the median is 0.012. This result is lower than the integration of the backward fraction of the Petzold phase function, 0.0183. Positively skewed and lognormal distributions are commonly observed in histograms of bio-optical variables [26]. We used a natural log transformation on the data to perform a parametric statistical analysis (assuming a normal distribution). Statistical descriptors such as the mean and standard deviation were estimated on the transformed data, and then back-transformed to obtain numbers that are on the same scale as the data. Transforming the backscattering ratios did not produce a normal distribution (e.g. it failed the Jarque-Bera test), but it did reduce the amount of skewness to 0.64.

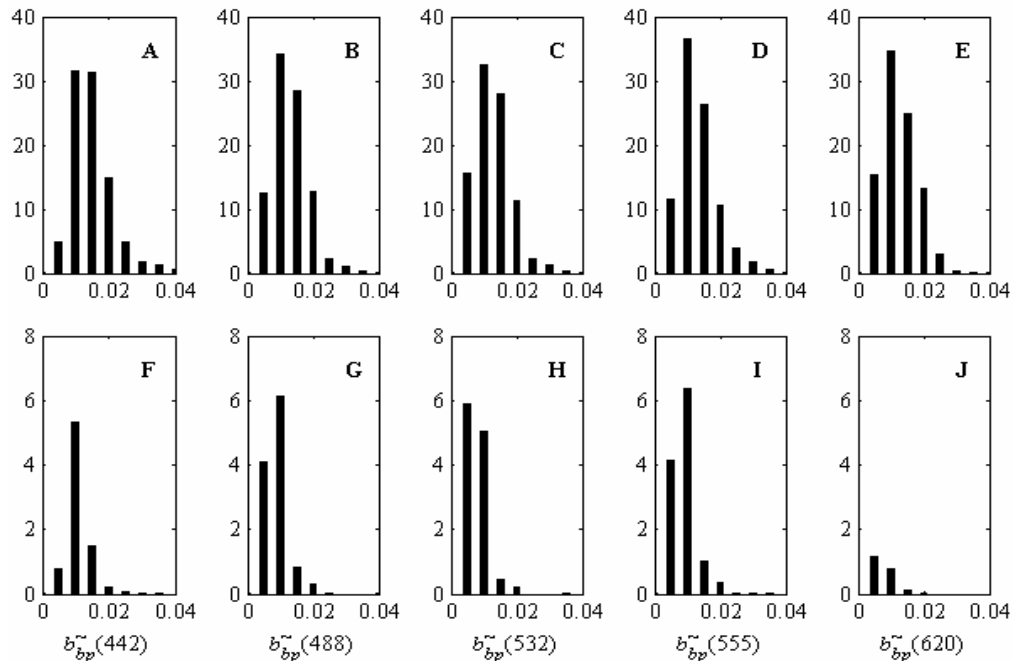


Fig. 1. (A – E) Histograms of particulate backscattering ratio measurements for the entire data set are plotted for each wavelength. Frequency values shown on the y-axes have been divided by 100.  $N = 9,154$  for each plot. (F – J) Particulate backscattering ratios that occur at or above one optical depth are plotted. (F) 442 nm,  $N = 797$ . (G) 488 nm,  $N = 1,149$ . (H) 532 nm,  $N = 1,154$ . (I) 555 nm,  $N = 1,193$ . (J) 620 nm,  $N = 212$ .

Table 2. Descriptive statistics of  $\tilde{b}_{bp}(\lambda)$  for the individual data sets

Data Set		442 nm	488 nm	532 nm	555 nm	620 nm	442 nm	488 nm	532 nm	555 nm	620 nm
GOC99A	Mean	0.0130	0.0126	0.0121	0.0114	0.0113	0.0100	0.0095	0.0087	0.0090	0.0086
	10 <sup>th</sup> percentile	0.0089	0.0081	0.0077	0.0077	0.0072	0.0074	0.0068	0.0063	0.0065	0.0061
	90 <sup>th</sup> percentile	0.0179	0.0185	0.0179	0.0167	0.0172	0.0139	0.0134	0.0118	0.0127	0.0130
MOCE-5	Mean	0.0153	0.0125	0.0133	0.0123	0.0129	0.0104	0.0080	0.0079	0.0083	0.0074
	10 <sup>th</sup> percentile	0.0100	0.0084	0.0086	0.0083	0.0083	0.0066	0.0051	0.0050	0.0053	0.0054
	90 <sup>th</sup> percentile	0.0250	0.0183	0.0213	0.0176	0.0201	0.0155	0.0119	0.0121	0.0132	0.0121
HY00	Mean	0.0131	0.0113	0.0103	0.0097	0.0096	0.0113	0.0091	0.0080	0.0077	0.0075
	10 <sup>th</sup> percentile	0.0094	0.0079	0.0067	0.0065	0.0061	0.0094	0.0066	0.0059	0.0056	0.0054
	90 <sup>th</sup> percentile	0.0213	0.0189	0.0172	0.0162	0.0161	0.0204	0.0190	0.0115	0.0104	0.0169
CL01	Mean	0.0184	0.0144	0.0139	0.0166	0.0145	0.0156	0.0111	0.0131	0.0187	0.0136
	10 <sup>th</sup> percentile	0.0098	0.0067	0.0068	0.0087	0.0081	0.0101	0.0054	0.0093	0.0150	0.0126
	90 <sup>th</sup> percentile	0.0360	0.0309	0.0298	0.0296	0.0234	0.0264	0.0209	0.0191	0.0236	0.0150
HY01	Mean	0.0129	0.0108	0.0102	0.0126	0.0110	0.0103	0.0076	0.0064	0.0085	0.0069
	10 <sup>th</sup> percentile	0.0074	0.0059	0.0056	0.0065	0.0061	0.0081	0.0054	0.0046	0.0051	0.0052
	90 <sup>th</sup> percentile	0.0224	0.0200	0.0194	0.0237	0.0208	0.0131	0.0108	0.0088	0.0124	0.0097

Statistics for the entire data set are shown on the left. Statistics for data within the first optical depth are shown on the right. The geometric mean is shown.

Spectral relationships were examined using Model-II linear regression [28]. We derived regressions of particulate backscattering ratios between wavelengths to establish whether or not the ratio varies spectrally. A significant deviation from a slope of one would indicate that there is spectral variation in the ratio. We chose 488-nm as the reference wavelength for plots to match previous work on global spectral IOP relationships [15]. We used the “least squares bisector” approach for the Model-II regressions [29]. In this method a Model-I robust linear least squares model is fit to both  $x$ -on- $y$  and  $y$ -on- $x$ , e.g.  $\tilde{b}_{bp}(488)$  vs.  $\tilde{b}_{bp}(442)$  and vice-versa. The slope of the Model-II regression is determined by bisecting the minor angle between the two Model-I regression slopes (Fig. 2). A robust model, which weights points

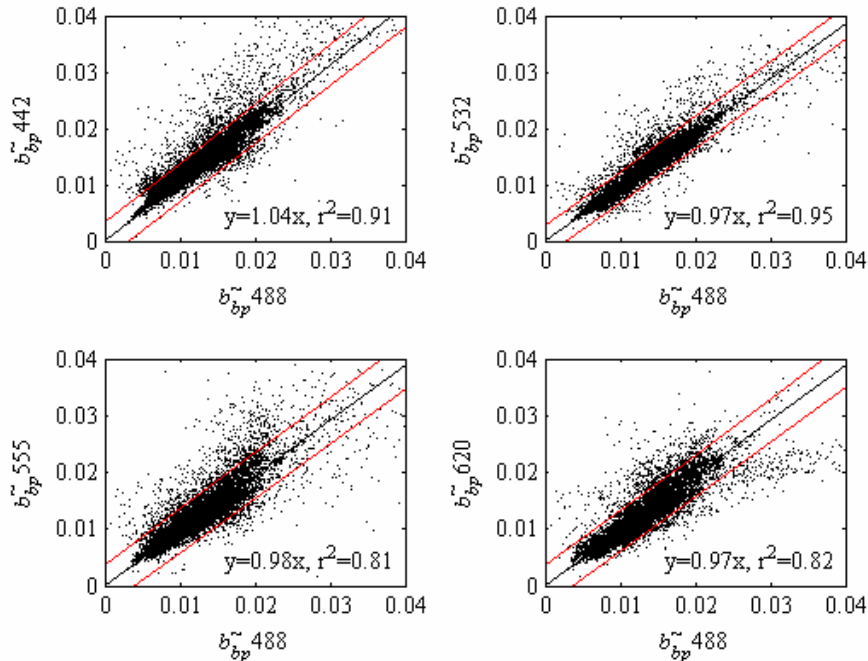


Fig. 2. Particulate backscattering ratio at 488 nm plotted versus the particulate backscattering ratio measured at four other wavelengths for the entire global data set. The Model II regression fits at each wavelength are shown with 90% confidence limits (red). The number of data points for each regression is 9,154.

close to the regression line more heavily than more distant points, was utilized to minimize the effect of outliers. We also centered the data by removing the mean value from all data points before performing the regression [30]. The y-intercepts retrieved from the Model-II regressions were all well below the magnitude of our measurement certainty ( $<0.0001$ ), and are therefore indistinguishable from zero. The slopes of the regressions varied between 0.97 and 1.04. The 90% confidence intervals for the regressions show that the slopes are not significantly different from one (Fig. 2).

The particulate backscattering ratio has a wide dynamic range (0.005 – 0.06), often varying by an order of magnitude in a single profile. This is reflected in the large standard deviations around the mean  $\tilde{b}_{bp}(\lambda)$  spectra shown in Fig. 3. Although plots of  $\tilde{b}_{bp}(\lambda)$  spectra for individual cruises show apparent spectral variation in their mean values, the variability between wavelengths is lower than the uncertainty in the estimate. Likewise, the variability between wavelengths in the combined data set is also much lower than the uncertainty in the estimation of the ratio. The results of the regressions, the level of uncertainty in the ratio, and the high standard deviations all point to the conclusion that there is no measurable difference between particulate backscattering ratios at the five wavelengths sampled, and we therefore find no statistically significant spectral dependence to the ratio.

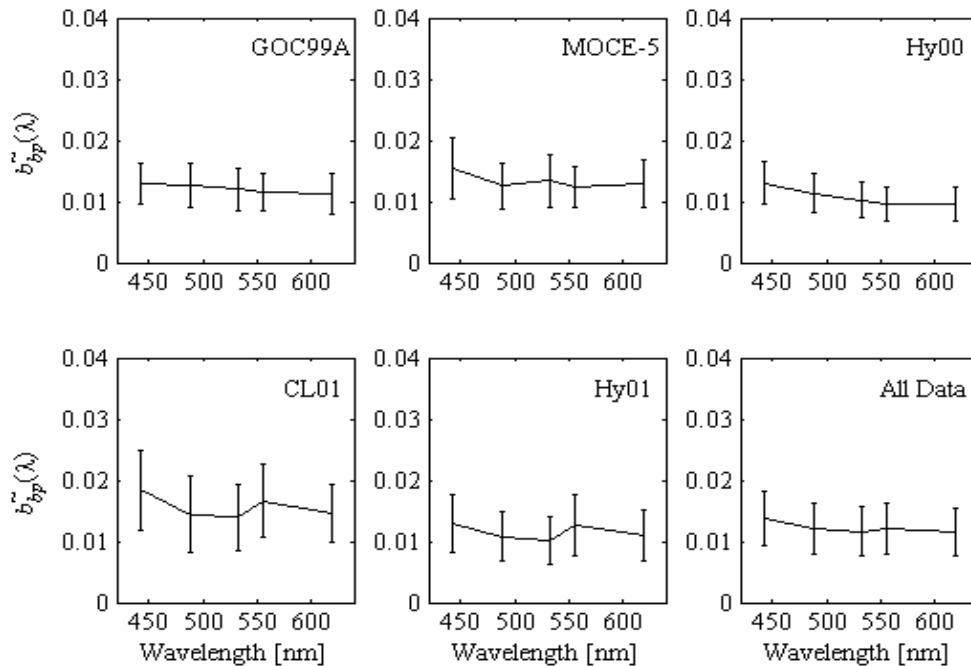


Fig. 3. Mean particulate backscattering ratio spectra for individual data sets, with one standard deviation shown for each data point. The spectra are as follows: GOC99A (top, left), MOCE-5 (top, middle), HyCODE 2000 (top, right), Crater Lake 2001 (bottom, left), HyCODE 2001 (bottom, middle), and the mean of all of the data sets (bottom, right).

#### 4. Discussion

The absence of spectral differences in the particulate backscattering ratio has been predicted by Mie theory [11] for populations of spherical, homogeneous particles that follow a Junge-type size distribution and have a constant refractive index, similar to that of phytoplankton, across all wavelengths. Previous work found between 4% and 10% variability between wavelengths in the backscattering ratio [13 and 12 respectively]. Our findings, using a much larger data set than previous analyses, exhibit the same result with regard to spectral

variability. This is illustrated by slopes not significantly different from one for linear regressions between five wavelengths of the ratio (Fig. 2).

An exception to this linear relationship occurred in the regression of backscattering ratios at 488- and 620-nm for backscattering ratios larger than 0.025. Data points where ratios fell below the regression line had  $c_p(\lambda)$ -slopes near zero. This can occur when the particle population does not follow the hyperbolic size distribution model, and is usually the result of a phytoplankton bloom [10]. Interestingly, the low  $c_p(\lambda)$ -slopes in these data are not coincident with high chlorophyll. Chami et al. [13] observed that the particulate backscattering ratio occasionally exhibited spectral variability between three wavelengths when there was high non-algal particle absorption, but the relationship was not systematic enough to describe mathematically. These exceptions illustrate that important deviations from flat  $\tilde{b}_{bp}(\lambda)$  spectra can occur under specific circumstances. However, data points divergent from the regressions were very rare in our data set, and removing them from the database did not significantly affect the slope of the regression.

The particulate backscattering ratio is, by construction, a concentration independent quantity, as it is the ratio of two optical parameters that to first degree co-vary with concentration. Instead, this ratio provides information about characteristics of the bulk particle population (e.g. particle composition, mean size, shape etc.). In previous studies it was found (based on theory and observations) that the backscattering ratio is sensitive to composition (organic content and particle size distribution) [6, 7]. In this regard, we examined the magnitude and variability of  $\tilde{b}_{bp}(\lambda)$  across various biogeochemical provinces. We did not have ancillary information from discrete water samples to determine the dominant particle types for all of the stations in the database. Instead, backscattering ratios were partitioned into groups according to chlorophyll concentration, beam attenuation, and combinations of the two parameters.  $\tilde{b}_{bp}(\lambda)$  values were also examined in the first optical depth of the water column to determine if mean surface values differ from generalized whole water-column values.

Since most phytoplankton groups exhibit a low backscattering efficiency [6, 31, 32], we expect to find low backscattering ratios in areas of high chlorophyll (and low proportions of mineral particles). To examine the relationship between chlorophyll and the particulate backscattering ratio we placed data into two groups, one with chlorophyll values between 0.02 and 2.0  $\mu\text{gL}^{-1}$ , and the other with chlorophyll greater than 2  $\mu\text{gL}^{-1}$ . We found that regions with low chlorophyll concentration exhibit higher backscattering ratios than areas with high chlorophyll (Fig. 4(A), black and green lines respectively). This result supports the approach taken in previous studies in which the magnitude of the backscattering ratio is approximated to first order by the chlorophyll concentration [33].

There was a weak relationship between chlorophyll concentration and the backscattering ratio in our data (Fig. 5, solid red line). The relationship is similar to those found in several previous studies [6, 10, 11, 33], despite the fact that these studies cover different ranges of chlorophyll concentration. For example, the chlorophyll concentration in our study ranged from undetectable to just over 12  $\mu\text{gL}^{-1}$ . Sullivan *et al.* [10] found a similar relationship between the particulate backscattering ratio and chlorophyll in a dataset that included a large set of high chlorophyll data points reaching up to 100  $\mu\text{gL}^{-1}$ . The relationship found here is described by the equation:

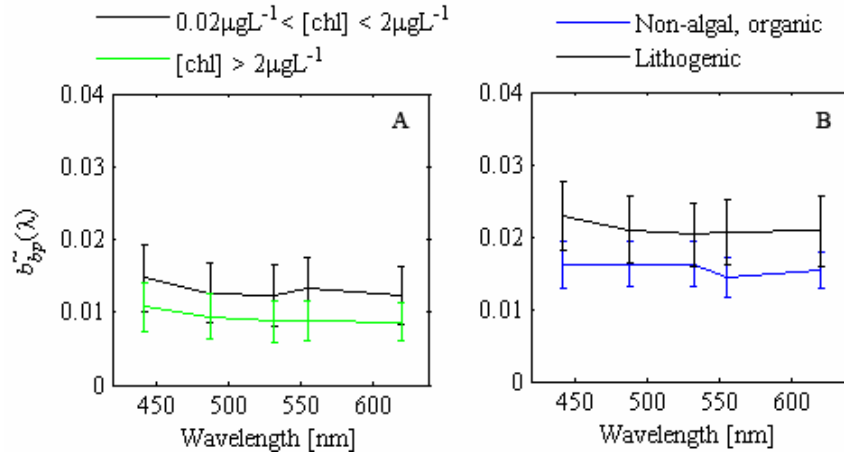


Fig. 4. Mean particulate backscattering ratio spectra for different biogeochemical provinces. One standard deviation is plotted on each mean. (A)  $b_{bp}(\lambda)$  ratios where chlorophyll concentration lies between  $0.02$  and  $2\mu\text{gL}^{-1}$  (black,  $N = 6,049$ ) and  $b_{bp}(\lambda)$  ratios where chlorophyll concentration is above  $2\mu\text{gL}^{-1}$  (green,  $N = 2,242$ ). (B)  $b_{bp}(\lambda)$  ratios where chlorophyll concentration is zero and where the particulate beam attenuation at  $650\text{ nm}$  is  $\leq 0.5\text{ m}^{-1}$  (blue,  $N = 772$ ) and  $b_{bp}(\lambda)$  ratios where chlorophyll concentration lies between  $0$  and  $0.5\mu\text{gL}^{-1}$  and where the particulate beam attenuation at  $650\text{ nm}$  is above  $1\text{ m}^{-1}$  (black,  $N = 18$ ).

$$\tilde{b}_{bp}(555) = 0.0121[\text{chlorophyll}]^{-0.125}; r^2 = 0.36. \quad (1)$$

However, below chlorophyll values of approximately  $2\mu\text{gL}^{-1}$  the particulate backscattering ratio is extremely variable, ranging from  $0.004$  to  $0.05$ , and chlorophyll concentration is no longer a good predictor of the ratio in our data. Twardowski et al. [6] found the same result, with large amounts of scatter in backscattering ratios at low chlorophyll values. Since phytoplankton exhibit relatively weak backscattering compared to lithogenic and non-algal material, we expect that other particles will contribute strongly to the magnitude of the backscattering ratio at low chlorophyll concentrations. The wide range of values observed reflects pervasive differences in bulk particle composition with changes in depth, water mass, and sampling location. The relationship between chlorophyll and the particulate backscattering ratio is slightly more robust within the first optical depth of the water column (Fig. 5, red dashed line). The relationship is described by the power-law model in Eq. (2):

$$\tilde{b}_{bp}(555) = 0.0074[\text{chlorophyll}]^{-0.042}; r^2 = 0.47. \quad (2)$$

The lower value of the exponent in the model compared to Eq. (1) is the result of lower backscattering ratio values at the surface, which are presumably dominated by phytoplankton with a low refractive index.

It is interesting to note that backscattering ratios often exceeded values predicted by models with 'typical' phytoplankton input parameters, even when chlorophyll was high. For values of the real refractive index typical of phytoplankton ( $1.04 - 1.06$  relative to water), and typical size distributions observed in the ocean, the Mie model predicts backscattering ratios between approximately  $0.5 - 1\%$  [11]. We observed values as high as  $0.02$ , or  $2\%$ , at chlorophyll concentrations as large as  $6\mu\text{gL}^{-1}$ , and ratios still as high as  $1.5\%$  at chlorophyll concentrations reaching  $12\mu\text{gL}^{-1}$ . This indicates that the ways in which phytoplankton deviate from the assumptions inherent in the Mie model may significantly increase their backscattering. For example, complex morphology [34] and internal structure [35] have been

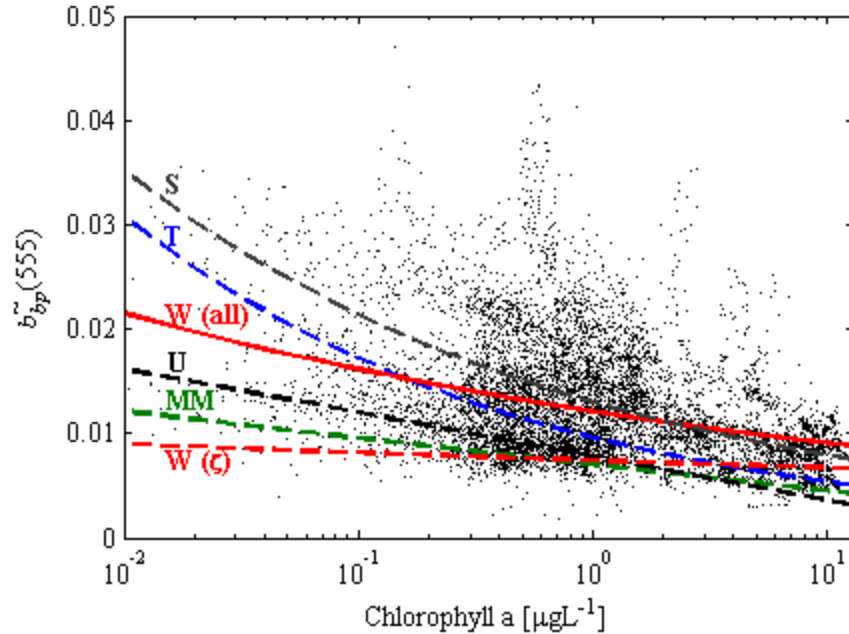


Fig. 5. The particulate backscattering ratio at 555-nm as a function of chlorophyll-a concentration [W(all)]. Curves showing the relationship based on models by Sullivan et al. [2006], Twardowski et al. [2001], Ulloa [1994], and Morel and Maritorena [2001] are identified as S, T, U, and MM respectively. The solid red line [W(all)] is the least-squares power-law fit to data in this study. The dashed red line [W( $\zeta$ )] is the least-squares power-law fit to the data above one optical depth.

shown to increase the proportion of backscattering relative to homogeneous particles with an equivalent spherical diameter.

Samples with low beam attenuation and no chlorophyll generally occur below the chlorophyll maximum and above the bottom boundary layer, somewhere in the middle of the water column. Under these circumstances the inherent optical properties are presumably dominated by non-algal material. We classify samples with a beam attenuation of less than  $0.5\text{m}^{-1}$  and no chlorophyll present to be ‘non-algal’ in nature. Previous work has hypothesized that very small non-algal particles are responsible for a large fraction of total backscattering in the ocean ([3], and references therein). We found that water masses dominated by such particles do exhibit high backscattering ratios, around 0.016 (Fig. 4(B), blue line). This result agrees well with previous work, which shows an increase in the backscattering ratio with depth as non-algal material becomes the dominant particle type in the water column [36]. Previous work has shown that spectral dependence occurs in the backscattering ratio when absorption by non-algal particles dominates the absorption signal [13]. We did not find the same result in our data, but it may be due to the different approach we took in categorizing non-algal particle populations (i.e. based on  $c_p(650)$  and chlorophyll instead of absorption-based techniques).

Lithogenic materials have a very high backscattering efficiency [6]. High values of both the particulate backscattering coefficient and the backscattering ratio are often seen in bottom boundary layers. Since our database of 234 profiles had a maximum depth range from 10 to 300 meters, using depth or depth from bottom was not a reasonable approach to deciphering which samples may be influenced by resuspended sediment. Profiles did not always reach proximity to the bottom, and even where the SlowDROP did reach the bottom a nepheloid layer was not always present. Instead, we classified ‘lithogenic’ samples according to chlorophyll (less than  $0.5\mu\text{gL}^{-1}$ ) and beam attenuation ( $c_p(650)$ ; greater than  $1\text{m}^{-1}$ ). Using these criteria we found that results agreed well with previous studies (Fig. 4(B), black line).

Samples that were categorized as being influenced by lithogenic particles had high backscattering ratios across all wavelengths, around 0.021, and represented the highest values in the dataset.

The backscattering ratio is an important parameter for remote sensing inversion algorithms [37]. To determine if surface values of the ratio differ significantly from mean water column values, we grouped data that was within the range of the first optical depth in all of our profiles. Figure 1(F) – 1(J) shows frequency distributions of  $\tilde{b}_{bp}(\lambda)$  at five wavelengths for these surface data. Compared to the entire data set, the surface values of  $\tilde{b}_{bp}(\lambda)$  are lower in magnitude, around 0.01 (see Table 2). This result has important implications when the backscattering ratio is employed in remote sensing algorithms, such as diver visibility algorithms designed to estimate the beam attenuation from inverted backscattering estimates [37].

## 5. Conclusion

The main objective of this research was to examine the distribution of the spectral particulate backscattering ratio *in situ* across several oceanic domains, both in terms of its absolute magnitude and its variability across visible wavelengths. We analyzed over nine thousand 1-meter binned data points for each of five wavelengths of the spectral particulate backscattering ratio. We found the maximum uncertainty in the backscattering ratio to be 15–20%. This result is largely due to the assumptions inherent in the conversion factor,  $\chi$ , from a single angle VSF measurement to the backscattering coefficient, and the propagation of uncertainties associated with using two instruments to compute the ratio. Within this measurement capability we found that there was no significant spectral dependence of the ratio. We observed rare instances of significant spectral deviation that were caused by particle populations that differ strongly from theoretical assumptions about their shape, composition, or size distribution. Spectral deviations in the particulate backscattering ratio have also been observed by others [13, 14], and merit further investigation. Different vertical biogeochemical provinces demonstrated qualitative differences in the backscattering ratio that agreed well with previous work. Mid-water regions with low chlorophyll exhibited higher backscattering ratios than surface regions with relatively higher chlorophyll. A power-law least-squares model was fit to the relationship between chlorophyll and the backscattering ratio. Though it was a weak relationship, it was similar to previous models. The relationship between chlorophyll and the ratio was more robust within the first optical depth of the water column, and had a lower slope exponent than the fit to the entire data set. Areas with a strong non-algal or lithogenic influence also showed elevated backscattering ratios compared with mean values. The highest ratios were associated with lithogenic material. Within one optical depth of the surface, the backscattering ratio averages 0.010, which is slightly lower than the mean of the data set as a whole. The lower backscattering ratio is associated with increased chlorophyll concentration near the surface.

## Acknowledgments

The authors thank two anonymous reviewers for helpful comments on the original manuscript. A. Whitmire was supported by the National Sea Grant College Program of the U.S. Department of Commerce's National Oceanic and Atmospheric Administration under NOAA grant number NA060AR4170010 (project number E/INT-61-IFP), and by appropriations made by the Oregon State legislature. The views expressed herein do not necessarily reflect the views of any of those organizations. Emmanuel Boss acknowledges grant N00014-04-1-0710 of the Environmental Optics and Biology program of the Office of Naval Research.